Crowding-induced transcriptional bursts dictate nucleosome and polymerase density profiles along genes

Aafke A. van den Berg and Martin Depken
Department of Bionanoscience, Kavli Institute of Nanoscience,
Delft University of Technology, Van der Maasweg 9
2629 HZ Delft, The Netherlands

During transcription, RNA polymerase competes for space on the DNA with other DNA binding proteins and higher order DNA structures acting as roadblocks. Though it is known that individual polymerases often slow down when forcing roadblocks, the effect of crowding on transcription as a whole is not clear. Based on quantitative theoretical modeling, we show that interactions with roadblocks induce a strong kinetic attraction between polymerases, causing them to self-organize into pelotons. Peloton formation explains observed nucleosome and polymerase density profiles close to the initiation site on highly transcribed genes, and how these densities depend on induction levels. At termination, pelotons translate into transcriptional bursts that dispaly the same characteristics as those observed *in vivo*. Our model thus unifies common spatial and temporal transcription patterns as arising from a non-specific interaction between roadblocks and polymerases. The generality of our model suggests that peloton formation might be ubiquitous in systems where molecular motors interact with dynamic roadblocks.

Introduction

On every scale, motility is a hallmark of life (Chowdhury et al., 2005; Hoyt et al., 1997). On the smallest scales, directed motion through the densely packed interior of cells is crucial for biogenesis, morphogenesis, and the delivery of vital cargo to distant parts (Howard, 2001). This motion is often carried out by large molecular complexes, powered along tracks by internal chemical reactions: polymerase and helicases move along DNA and RNA, ribosome along RNA, myosin along actin filaments, and dynein and kinesin along microtubules, to name but a few. The time requirements on these processes are in some cases so detailed that even fluctuations in activity appear molded by natural selection (Raj and van Oudenaarden, 2008). On top of the general scarcity of free space in the cell (Goodsell, 2009), many of the molecular machines driving translocation also have to deal with large amounts of obstacles along their path (Finkelstein and Greene, 2013) (**Figure 1 A-D**). Strikingly, over 80% of the DNA in eukaryotes is covered by nucleosomes (Lee et al., 2007), and it is then hardly surprising that overall transcription levels correlate *negatively* with nucleosome densities on genes (Cole et al., 2014; Lee et al., 2004, 2007; Shivaswamy et al., 2008). More surprising might instead be the fact that local polymerase and nucleosome densities correlate *positively* along heavily transcribed genes lacking promotor-proximally stalled polymerases: for the first few hundred base pairs after initiation, both the densities of nucleosomes and polymerases increase (Cole et al., 2014; Shivaswamy et al., 2008; Weiner et al., 2010). Though transcription lies at the heart of molecular biology (Crick, 1970), it is still not clear how this dynamic process is shaped by the most basic, ubiquitous, and non-specific interactions with the crowded environment of the cell.

With the aim to understand the effects of non-specific crowding interactions for transcription in dense environments, we construct a general theoretical model that quantitatively describes stochastic motors interacting with dynamic roadblocks. We show that roadblocks induce motors to gradually reorganize into pelotons through a phenomenon loosely analogous to drafting in racing sports (Trenchard, 2015). Relying on non-specific interactions alone, our model gives a parsimonious explanation for how nucleosome and polymerase densities can be globally anti-correlated, and still increase together along heavily transcribed genes (Cole et al., 2014). Additionally, the model offers a kinetic explanation for the clustering of polymerases seen in Miller spreads (Albert et al., 2011; Harper and Puvion-Dutilleul, 1979; Laird and Chooi, 1976; Mcknight and Miller, 1979). Roadblock induced peloton formation during the elongation phase also gives rise to a so-far unrecognized type of transcriptional bursts (Golding et al., 2005), which captures the experimentally observed dependence of burst parameters on transcription levels in *Escherichia coli* (So et al., 2011). Nucleosomes could similarly induce transcriptional bursts in eukaryotes (Kaern et al., 2005), and to facilitate future experimental testing we give quantitative predictions of how nucleosome and polymerase densities, as well as transcriptional burst parameters, depend on translocation rates, gene lengths, initiation rates, and nucleosome turnover times. As our model is based on general principles, it might also be describe motor and obstacle interactions in many other biological systems (**Figure 1 C and D**).

Results

The theoretical modeling of stochastic and driven molecular traffic on one-dimensional tracks has a long history in biology, starting almost half a century ago with the introduction of the Totally Asymmetric Simple Exclusion Process (TASEP) (MacDonald et al., 1968). The TASEP is defined as motors hopping stochastically along a one-dimensional lattice, moving only if the track just ahead is empty. Coupling this simple bulk rule to injection and extraction of motors at the boundaries gives rise to rich dynamical behavior, and the model has been modified and extended to describe a wide range of physical and biological systems (Blythe and Evans, 2007; Dobrzynski and Bruggeman, 2009; Klumpp, 2011; Klumpp and Hwa, 2008; Kunwar et al., 2004; Parmeggiani et al., 2004; Schadschneider et al., 2011).

A minimal model of motors interacting with roadblocks

To capture motor and roadblock interactions, we consider a system (**Figure 1 E**) for which: i) motors move stochastically in one direction along a track, ii) motors cannot overtake each other, iii) roadblocks dynamically appear and disappear from the track, iv) roadblocks immediately ahead of a motor impede the motion of the motor, and v) a passing motor temporarily removes a roadblock. A range of biological systems, a few of which are illustrated in **Figure 1 A-D,** likely satisfy the model criteria i)-v) under certain conditions.

The Bus-Route Model (BRM) (Loan et al., 1998) (**Figure 2 A**) is a simple idealized model realizing the above criteria on a circular track and with motor and roadblock sizes equal to the motor step size. The BRM has been solved in the mean-field limit (Loan et al., 1998), but this solution does not apply to the physiologically more relevant situation with large motor and roadblock sizes compared to the motor step, and motors that enter and leave the track at specific sites. As any microscopic model will at best approximate the biological system studied, we will lose little precision by taking a heuristic approach to understanding the dynamics. Instead, taking such an approach allows us to capture the dominant behavior of the wide class of systems satisfying condition i)-v). To this end, let τ be the roadblock-DNA binding equilibration time, and δ_{rb} and δ_{m} be the footprint of roadblocks and motors respectively, both measured in units of the motor step. To build intuition for the phenomenology of motor-roadblock-track interactions, we first investigate the dynamics in the bulk of the track, far away from boundaries.

A hierarchy of TASEPs controls the dynamics

The roadblock occupancy varies depending on the roadblock binding dynamics and motor-roadblock interactions. Consider the two limits of rare and ubiquitous roadblocks: in the former limit, the dynamics should approach that of the TASEP with the motor hopping rate set by the rate of hopping into empty sites; in the latter limit, the dynamics should approach that of a TASEP with a motor hopping rate set by the rate of hopping into a site occupied by a roadblock. In either limit, the exact solution of the TASEP (Derrida et al., 1993) gives a geometric distribution of gap sizes g between adjacent motors (see **Equation (7)** in **Materials and Methods**). In **Figure 2 B** and **C** we show kymographs and gap-size distributions generated by Monte Carlo simulations (see **Materials and Methods**) of the BRM (Loan et al., 1998). As expected, ubiquitous (left panel **Figure 2 B** and **C**) or sparse (right paned **Figure 2 B** and **C**) roadblocks result in gap-sizes distributions that are approximately geometrical.

For intermediate roadblock densities, the situation is subtler. Motors that are slowed down by roadblocks induce trailing traffic jams, while the gap to the motor ahead increases. With a gap opening up ahead, the motors grow more likely to encounter roadblocks deposited in the gap, and the jams stabilize into moving pelotons. Defining a peloton as being a group of motors with no interspersing roadblocks, a peloton can split at any position due to the binding of a roadblock, and the rate at which this happens should be roughly proportional to peloton size. Pelotons can also merge, but with a rate largely independent of peloton size. In the steady state, when the merging and splitting rates balance, we therefore expect pelotons to have a well-defined typical size. Furthermore, the merging and subsequent splitting of pelotons can be seen as an effective steric repulsion between pelotons, much like the interaction between motors in the original TASEP. The steady-state system can therefore be taken to be a superposition of two steady-state TASEP models: the intra-peloton TASEP (ipTASEP) originating from motor dynamics within pelotons, and the trans-peloton TASEP (tpTASEP) originating in the dynamics of the pelotons themselves. This hierarchical picture is confirmed in the middle panels of **Figure 2 B** and **C**, where we show a kymograph and a double-geometric gap distribution (one geometric distribution for each TASEP) for intermediate roadblock coverage in the BRM.

Stable pelotons and a heuristic solution of the TASEP hierarchy in the bulk

Due to the finite size and equilibration time of roadblocks, there is a region without roadblocks behind every moving motor. We will refer to this region as the roadblock shadow, and estimate its size as $\Delta = v^{\text{bulk}}\tau + \delta_{\text{rb}}$ (**Figure 2 A**). The term $v^{\text{bulk}}\tau$, with v^{bulk} being the average motor velocity in the bulk, captures the average distance traveled by a motor during the equilibration time of roadblocks, and δ_{rb} accounts for that a roadblock must first fit physically between motors before it can bind. We define gaps between pelotons as being filled with roadblocks, and thus to typically be larger than the roadblock shadow. Conversely, we take gaps within pelotons to be devoid of roadblocks, and thus they are typically smaller than the roadblock shadow. We denote the effective motor hopping rate into gaps without roadblocks as the intra-peloton hopping rate k_{ip}, and the rate of hopping into gaps with roadblocks as the trans-peloton hopping rate k_{tp}. In **Materials and Methods** we show that knowing the density of motors along the track $\rho_{\text{m}}^{\text{bulk}}$ we can predict the dynamics state of the system as long as $(k_{\text{ip}}/k_{\text{tp}})^{\Delta}$ is large, which we refer to as the stable peloton regime (SPR). The condition for the stable pelotons can intuitively be seen as combining the strength of the interaction between motors and roadblocks ($k_{\text{ip}}/k_{\text{tp}}$) and its range ($\Delta$). Due to the SPR conditions exponential dependence on the roadblock shadow size, we expect physiological systems where the roadblock size is substantially larger then the motor step to always be in the SPR.

In **Figure 3** we illustrate the relationships derived for various observables and check our arguments against simulations of the BRM. In **Figure 3 A-D** we show the effect of varying the trans-peloton hopping rates for long roadblock equilibration times. As predicted by our analytical arguments (see **Materials and Methods**), up to a critical motor density ρ_1 the velocity remains approximately constant (**Figure 3 A**)**,** and the total current of motors grows linearly with the motor density (**Figure 3B**), while the roadblock occupancy decreases linearly with motor density (**Figure 3 C**). At the critical density, and long before the track is completely covered by motors, all roadblocks are evicted. For motor densities above the critical density, the velocity and motor current follows the relationship for the TASEP without roadblocks (the ipTASEP) (for details see **Materials and Methods**) (**Figure 3 A and B**). In **Figure 3 D** we plot the typical peloton size up to the critical density, after which whole system acts as one large roadblock-excluding peloton. In **Figure 3 E-H** we vary the roadblock equilibration times. For rapid roadblock equilibration (red curves **Figure 3 E-H**) the roadblock shadow is small, gaps are largely filled with roadblocks, and the system is well described by a single TASEP with roadblocks in every gap (the tpTASEP) (dashed line in **Figure 3 E**). In this regime, the total density of roadblocks decreases weakly with motor density (red curve **Figure 3 G**), as roadblock shadows are small and the motor footprints are all that excludes the roadblocks. For intermediate roadblock equilibration times (the blue curves in **Figure 3E-H**) the roadblock shadow is larger, resulting in peloton formation, a velocity that is less sensitive to motor density, and a system that is better at evicting roadblocks. The breakdown of our predictions for roadblock densities and peloton size in the case of fast roadblock binding (red and blue curves in **Figure 3 G** and **H**) is not surprising given that we here have small enough roadblock shadows to push the system outside the SPR.

Motor and roadblock reorganization close to the initiation site

In transcription, initiation generally controls transcription levels (Cooper, 2000) and the state of the system in the beginning of the gene has the potential to influence the overall transcription levels (Jonkers and Lis, 2015). To describe this situation with our model, we consider open systems at low enough motor densities that initiation controls the overall flux of motors on the track. We also here consider the SPR, where pelotons are stable, and two motors that meet, practically stay together indefinitely.

For eukaryotic transcription, the initiation site is kept free of nucleosomes when a gene is active (Lee et al., 2007; Yuan, 2005). We also assume the initiation site in our model to be devoid of roadblocks, and that motors attempt to initiate with rate k_{in}. As they initiate, some of the motors will have roadblock just ahead of them, and some will not. Motors unhindered by roadblocks catch up with motors slowed down by roadblocks (see schematic kymograph in **Figure 4 A** upper panel), and motors collect into pelotons. As motors are absorbed into pelotons, the average velocity goes down, and as a consequence the motor density goes up (**Figure 4 A** lower panel), all while simultaneously also leaving more room available for roadblocks as roadblock shadows start to overlap. After the initial pelotons are formed, these will continue to evolve towards the bulk peloton size through a merging process described by diffusion-limited coagulation (Murthy and Schutz, 1998). Relaxation in such systems slows down drastically over time (referred to as aging in the physics literature), and we do not expect to see any appreciable evolution of the initially formed pelotons over a finite track (such as a gene). In **Materials and Methods,** we show that when initiation controls the overall level of motor activity, the average number of motors in the peloton grows over the initial portion of the track as

$$\langle n_{\text{p}}(x)\rangle = \langle n_{\text{p}}\rangle^{*} - \left(\langle n_{\text{p}}\rangle^{*} - 1\right)e^{-x/x^{*}}. \tag{1}$$

Here x^{*} is the typical distance over which the pelotons are formed, and $\langle n_{\text{p}}\rangle^{*}$ is the average number of motors in a fully formed peloton. The formation of pelotons drives the evolution of motor and nucleosome densities, as well as motor velocity, over the distance x^{*}. In **Materials and Methods** we give the general relations for $\langle n_{\text{p}}\rangle^{*}$ and x^{*} in terms of the microscopic model parameters, but for simplicity we here give the physiologically relevant limit where initiation rates are low enough that the system is initiation limited and motors do not interact much until they collect into pelotons,

$$\langle n_{\text{p}}\rangle^{*} \approx 1 + k_{\text{in}}\tilde{\tau}, \quad \tilde{\tau} = \Delta / k_{\text{tp}} = \tau + \delta_{\text{rb}} / k_{\text{tp}}, \quad x^{*} \approx \frac{\tilde{\tau}}{(1/k_{\text{tp}} - 1/k_{\text{ip}})} \cdot \frac{1/k_{\text{in}}\tilde{\tau}}{\ln\left(1 + 1/k_{\text{in}}\tilde{\tau}\right)}. \tag{2}$$

The new timescale $\tilde{\tau} = \Delta / k_{\text{tp}}$ is the time needed for a motor to clear the roadblock shadow. As it is often easier to experimentally measure relative changes, we report the relative change from initiation, indicated by the superscript 'in', to the point where pelotons are fully formed, indicated by the superscript *,

$$\frac{\rho_{\text{m}}^{*} - \rho_{\text{m}}^{\text{in}}}{\rho_{\text{m}}^{*}} = \left(1 - \frac{k_{\text{tp}}}{k_{\text{ip}}}\right)\frac{k_{\text{in}}\tilde{\tau}}{1 + k_{\text{in}}\tilde{\tau}}, \quad \frac{v^{*} - v_{\text{in}}}{v^{*}} = -\left(\frac{k_{\text{ip}}}{k_{\text{tp}}} - 1\right)\frac{k_{\text{in}}\tilde{\tau}}{1 + k_{\text{in}}\tilde{\tau}}, \quad \frac{\rho_{\text{rb}}^{*} - \rho_{\text{rb}}^{\text{in}}}{\rho_{\text{rb}}^{*}} = \frac{k_{\text{in}}\tilde{\tau}}{e^{\delta_{\text{rb}}/x^{*}} + k_{\text{in}}\tilde{\tau}}. \tag{3}$$

From this we see that both the motor and the roadblock density grow along the track, while the motor velocity decreases. Further we see that all relative changes along the track grow in magnitude with the initiation rate, but that the effect saturates around $k_{\text{in}} \sim 1/\tilde{\tau}$ for motor-density and velocity changes, while the roadblock density saturates later, around $k_{\text{in}} \sim e^{\delta_{\text{rb}}/x^{*}}/\tilde{\tau}$. Interestingly, we see that the total shift in motor density and velocity along the track is set solely by the ratio of motor stepping rates with and without roadblocks ahead.

In **Figure 4 B** we illustrate how the relative change in motor density is affected by the motor initiation rate, comparing the expressions derived in **Materials and Methods** to simulations of the BRM. For slow initiation ($k_{\text{in}}\tilde{\tau} < 1$, green arrow in **Figure 4 B**), a roadblock typically binds between every two initiating motors. Therefore, fully formed initial pelotons are typically of size one, giving only a marginal motor density change along the track (**Equation (3)** and top density profile of **Figure 4 D**). For faster initiation ($k_{\text{in}}\tilde{\tau} > 1$, red arrow **Figure 4 B**), multiple motors bind before a roadblock rebinds to the start of the track, fully formed pelotons are larger than one, and we have a substantial increase in motor density as we move away from the initiation site (lower density profile of **Figure 4 D**). In **Figure 4 C** we compare our prediction for the distance over which pelotons form, x^*, to estimates extracted by fitting an exponential relaxation to the density profiles generated by simulations of the BRM. It is striking that our at times crude approximations still capture the simulated data quantitatively without any adjustable parameters.

From pelotons to bursts

The peloton-forming dynamics of our model will manifest as burst of motor activity if viewed from a specific position. In **Materials and Methods** we relate the bursts of motor activity in our microscopic model to the phenomenological two-state model usually used to describe transcriptional bursts (**Figure 4 E**) (Golding et al., 2005). In the two-state model, the system switches between an on-state with production rate k_{tr}, and an off-state where nothing is produced. The off-state switches to the on-state with rate k_{on}, and back again with rate k_{off}. Though we present the full form of how the effective burst parameters depend on microscopic parameters in **Materials and Methods**, we here give the physiologically relevant limit where the motors are large compared to the motor step size, and the initiation rate is low compared to the motor stepping rate,

$$k_{\mathrm{tr}} = \frac{k_{\mathrm{in}}\tilde{\tau}}{1+k_{\mathrm{in}}\tilde{\tau}}\frac{k_{\mathrm{tp}}}{\delta_{\mathrm{m}}}, \quad k_{\mathrm{off}} = \frac{1}{1+k_{\mathrm{in}}\tilde{\tau}}\frac{k_{\mathrm{tp}}}{\delta_{\mathrm{m}}}, \quad \text{and} \quad k_{\mathrm{on}} = \frac{1}{\tilde{\tau}}. \tag{4}$$

While the apparent on rate is independent of the induction level, and the production rate in the on-state is insensitive to the initiation rate at high induction, the off rate decreases indefinitely with the initiation rate. It should also be noted that as long as the track is longer than x^* (which should be the case for transcription), **Equation (4)** applies, and the burst characteristics does not depend on the length of the track. **Equation (4)** gives the quantitative dependence of the effective burst parameter on the systems microscopic properties, and is therefore well suited for testing our model against experimental data (see **Discussion**).

Transcription on heavily transcribed inducible genes

Now that we understand the general effects of non-specific interactions between motors and roadblocks, we proceed to analyze our model with microscopic parameters estimated for inducible genes in eukaryotes. The considerations are complicated by that nucleosome assembly and disassembly are not single step processes, as a tetramer and two dimers come together to make the full histone octamer contained in the nucleosome core particle. *In vitro* studies have shown that a single polymerase only removes the histone dimer (Angelov et al., 2006; Belotserkovskaya et al., 2003; Kireeva et al., 2002), while a second polymerase can dislodge the remaining hexamer (Kulaeva et al., 2010). These *in vitro* results broadly agree with the *in vivo* observations that the density of histone dimers decreases strongly with transcription intensity genome wide, while an increased exchange and depletion of all core histones is only observed on highly transcribed genes (Cole et al., 2014; Dion et al., 2007; Jamai et al., 2007; Kristjuhan and Svejstrup, 2004; Lee et al., 2004; Rufiange et al., 2007; Thiriet and Hayes, 2005). As we are only expecting pelotons to form when several polymerases occupy the gene simultaneously, we compare our model to the experiments tracking highly expressed genes (see **Table 1**). Importantly, we do not model the situation where transcription is paused by promoter-proximally paused polymerases, but only genes where initiation is both active and non-paused (Core et al., 2008). Being interested in highly transcribed genes, we also assume that the roadblocks consist of histone hexamers that get dislodged by a passing polymerase.

As the bulk dynamics will never be reached over a finite gene length (see **Material and Methods**), we compare the predictions of our theory near the initiation site to simulations of the open system in **Figure 5**. In our simulations we assume that the motors are only impeded at the nucleosome dyad, since this forms the largest obstacle for RNA polymerase (RNAP) II translocation (Hodges et al., 2009). We consider the initiation rates $k_{\text{in}} = 0.6\ \text{pol/min}$ and $k_{\text{in}} = 3.0\ \text{pol/min}$, where both rates correspond to highly induced genes, and the highest rate is chosen to match the maximal estimate of initiation rates on yeast genes (Pelechano et al., 2010). It is known that histones redeposit after the passages of RNAP on a sub minute time scale (Schwabish and Struhl, 2004), and as it takes about a minute to clear space for a roadblock (see **Table 1**), this indicates that the nucleosome shadow is dominated by the roadblock size, and we take $\Delta \approx \delta_{\text{rb}}$ in the analytical theory.

Note how our theory captures the dynamics quantitatively without any free parameters, and utilizing only a small set of microscopic input parameters. As predicted by **Equation (1),** we see that pelotons grow over the first few hundred base pairs after initiation (**Figure 5 A** and **C**). The peloton growth in turn means that the density of RNAP and nucleosomes near the initiation site is lower than further into the gene, while the velocity decreases as we move away from initiation (**Figure 5 B** and **D**). After this point, the RNAP and nucleosome densities, as well as RNAP velocities, remain virtually constant throughout the bulk of the gene. In **Table 2** we give an overview of the predicted values of several observables, including burst parameters.

Discussion

With the aim of describing transcription in the crowded environment of the cell, we have introduced a general model that potentially captures a large class of systems where molecular motors interact with dynamic roadblocks (see for example **Figure 1 A-E**). Based on a physical mechanism reminiscent of drafting in racing sports, we show how the most basic and non-specific interactions between motors and roadblocks give rise to an effective kinetic attraction between motors. This attraction induces the motors to spontaneously reorganize into pelotons as they move into the track, and when the motors reach the terminus, they do so in bursts.

Peloton formation has been observed *in vivo*

There was early evidence from Miller spreads suggesting polymerases might cluster on genes (Albert et al., 2011; Harper and Puvion-Dutilleul, 1979; Laird and Chooi, 1976; Mcknight and Miller, 1979), and during the review process of this manuscript there emerged direct real-time evidence of polymerase 'convoys' on HIV-1 and POLR2A genes in HeLa cells (Tantale et al., 2016). As we predict, the typical distance between polymerases within such a convoy is too small for a nucleosome to bind, the distances between convoys are geometrically distributed, and the convoys include several polymerases (see **Table 2**). The excellent agreement between our predictions and these experimental observations suggests that peloton formation of polymerases through interactions with nucleosomes could be the underlying mechanism driving the formation of the observed polymerase 'convoys'.

Predicted density profiles agree with observations on heavily transcribed genes in yeast

Our model also gives parsimonious explanations for several recent *in vivo* experimental observations pertaining to density profiles of polymerases and nucleosomes along inducible genes. For highly transcribed genes without promotor-proximally paused polymerases, both polymerase and nucleosome densities are depleted for the first few hundred base pairs after initiation (Cole et al., 2014; Core et al., 2008). Though there are many specific interactions that could give rise to nucleosome and polymerase depletion in the beginning of genes (Jonkers and Lis, 2015), the fact that this is a general property of heavily transcribed genes (Cole et al., 2014; Dennis et al., 2009) suggests a non-specific mechanism. Indeed, our model accurately predicts the occurrence and extent of such depletion without evoking any specific interactions (see **Equation (2)** and **(3),** as well as **Figure 5** and **Table 2**). Though already correctly predicting a pausing-index (relative polymerase density within the promotor-proximal region compared to the bulk) below one for highly transcribed genes (Core et al., 2008), our model could be further tested by correlating changes in the pausing-index with changes in the microscopic parameters entering into **Equation (3).**

Interestingly, a nucleosome-free region at the start of genes (Cole et al., 2014; Shivaswamy et al., 2008; Weiner et al., 2010) has been suggested to increase the accessibility of transcription factor binding sites close to the initiation site, thereby increasing the potential for transcriptional regulation (Shivaswamy et al., 2008; Weiner et al., 2010). Our model thus suggests that nucleosome depletion could be a transcriptional epiphenomenon that has been coopted/adapted to allow for a greater regulatory response.

The predicted increase of the polymerase density along the gene coincides with a *decrease* in the elongation rate (see **Figure 5 B** and **D**). Genome wide GRO-seq experiments on active genes, on the contrary, have shown that the elongation rate *increases* over the first 15 kbp (Danko et al., 2013). The velocity increase in these GRO-seq experiments was likely caused by elongation factors, cooperation of polymerases, and/or histone modifications (Danko et al., 2013)—mechanisms not included in this model. Though it would be interesting to see how such mechanisms modulate the formation of pelotons, the observed increase of the elongation rate takes place over distances much longer than the few hundred base pairs over which pelotons form (see **Table 2**), and we do not expect our quantitative results to change close to the promoter.

Characteristics of crowding induced transcriptional bursts agree with *in vivo* observations

Though bursts in RNA production has been observed in both prokaryotes (Chong et al., 2014; Golding et al., 2005) and eukaryotes (Chubb et al., 2006; Raj et al., 2006), the origin is unclear, and usually modeled phenomenologically as depending on a promoter that turns on and off (Li et al., 2011; Raj and van Oudenaarden, 2008). Our model, on the contrary, quantitatively predicts that under conditions of molecular crowding, transcriptions should always be expected to be bursty on heavily transcribed genes—even if the promoter is constantly on. Several properties of the predicted bursts agree quantitatively with experimental observations. First, the pelotons are completed over a few hundred base pairs, which is shorter than the most genes. Therefore the predicted burst size is independent of gene length, agreeing with observations in yeast (Zenklusen et al., 2008). Secondly, the predicted time between production is on a sub-minute time scale (see **Table 2**), which falls within the experimentally observed range (Zenklusen et al., 2008). It is interesting to note that multi-scale bursting was recently reported (Tantale et al., 2016), which could very well originate in a premotor turning on and off on long timescales, while pelotons still form during elongation, giving rise to bursting on shorter timescales. Thirdly, our model predicts that only the apparent burst duration should be sensitive to transcription intensity at high induction (see **Equation (4)**), agreeing with the behavior reported for transcriptional bursting in *Escherichia coli* (*E. coli*) (So et al., 2011).

Though there are many DNA binding proteins in *E. coli* (Luijsterburg et al., 2008), another interesting candidate for producing bursts is DNA supercoiling. Due to the helicity of DNA, transcribing polymerases are known to induce positive supercoils ahead and negative supercoils behind (Liu and Wang, 1987). Such supercoils slow down the RNAP (Chong et al., 2014), and will in the steady state extend some finite distance in front and behind a polymerase. As negative supercoils spontaneously annihilate with positive supercoils, any DNA between two close by polymerases will have a lower supercoiling density the closer together the polymerases are (**Figure 1 B**). With a lower supercoiling density ahead, a trailing polymerase will move faster than a leading polymerase, and all the conditions for peloton formation as described by our model (**Figure 1 D**) are fulfilled. Our general mechanism of burst generation is thus connected to the mechanism suggested as a source of transcriptional bursting observed in bacteria, where a buildup of supercoils in torsional constrained plasmids was shown to lower transcription levels until the supercoils were released (Chong et al., 2014). Importantly though, our model does not require the DNA to be torsional constrained as the supercoiling density around RNAP is set by the supercoils diffusivity (van Loenhout et al., 2012) and a balance between supercoil creation and release.

Transcriptional bursts and polymerase backtracking

To our knowledge, there are only two previous theoretical studies suggesting that bursts are created during elongation (Dobrzynski and Bruggeman, 2009; Voliotis et al., 2008). In both cases, intrinsic polymerase pausing through backtracking (Shaevitz et al., 2003) was suggested as the source. However, backtracking is unlikely to produce bursts, as it does not induce an effective attraction between polymerases, but rather an effective repulsion: interaction with a trailing polymerases is known to help terminate backtracks of a leading polymerase, and so speeds it up; interaction with a leading polymerase increases the chance of pausing in a trailing polymerase (Jin et al., 2010; Kulaeva et al., 2010), and so slows it down. Polymerases thus dynamically repulse each other, and jams induced by backtracks are unstable, and should typically dissolve before termination. Instead, we have shown that the interaction with roadblocks induces a persistent effective attraction between polymerases, resulting in a fast buildup of stable pelotons as polymerases move through the gene, terminating in bursts.

Conclusion and outlook

Our model points to a single source for a wide range of observed phenomena, and has the potential to reshape our understanding of how transcribing polymerases and nucleosomes organize spatially and temporally in physiologically crowded environments. Only by first understanding this organization will it be possible to fully understand the action of elongation factors and other important cellular responses acting on the elongation phase of transcription. It would therefore be interesting to further test our model against dedicated experiments. Confirmation could be sought by expanding on the experiments reporting polymerase ‘convoys’, manipulating/screening the limited set of effective parameters that controls the spatial and temporal evolution of the system (**Equation (3)** and **(4)**). For example, the parameter that controls the saturation ($k_{\mathrm{in}}\tilde{\tau}$) could be manipulated by changing the transcription initiation rate, or through histone modifications that change the nucleosome-rebinding rate to DNA. Further, the parameter that controls the magnitude of change in both density and velocity profiles ($k_{\mathrm{tp}} / k_{\mathrm{ip}}$) can be controlled by various elongation factors (Jonkers and Lis, 2015), or histone modifications (Bintu et al., 2012) that change the nucleosomes affinity to DNA. Only through further experiments will it be possible to determine the extent to which the non-specific interactions we consider unify the spatiotemporal organization of nucleosomes and polymerases during transcription.

Materials and methods

We here give the derivations and arguments left out in the **Results** section. For brevity we will here only keep the "b" of "bulk" in the subscript, for example writing v^{b} instead of v^{bulk}.

Heuristic solution for of the hierarchical TASEP model

The average TASEP motor velocity

For the TASEP, gap sizes g are geometrically distributed as (Derrida et al., 1993),

$$P_{\text{TASEP}}(g;a) = (1-a)a^{g}, \tag{5}$$

for some constant $a<1$. Unless a motor is blocked by another motor ($g=0$), it will hop forward with rate k, and the average velocity of motors can be calculated as

$$v^{\text{b}} = k\sum_{g=1}^{\infty} P_{\text{TASEP}}(g;a) = ka. \tag{6}$$

From this it follows that $a = v^{\text{b}}/k$, and we can write

$$P_{\text{TASEP}}(g;v^{\text{b}}/k) = (1-v^{\text{b}}/k)(v^{\text{b}}/k)^{g}. \tag{7}$$

Intra- and trans-peloton gap sizes

The inclusion of dynamic roadblocks will split the motor dynamics into an intra-peloton and a trans-peloton TASEP describing gap sizes below and above the roadblock shadow Δ. In line with our heuristic argument, we assume there to be no roadblocks within a peloton. Apart from the leading motor, all motors within a peloton thus attempt to hop forward with rate k_{ip}. The pelotons themselves are controlled by the leading motor, which faces a trans-peloton gap filled with roadblocks and thus attempts to hop forward with rate k_{tp}. Assuming that the gap-size distribution is geometric both below and above the roadblock shadow, we can now write our normalized heuristic gap-size distribution for the intra- and trans-peloton regimes as

$$\begin{aligned}
P_{\text{ip}}(g;v^{\text{b}}/k_{\text{ip}}) &= \frac{(v^{\text{b}}/k_{\text{ip}})^{g}}{\sum_{g=0}^{\Delta-1}(v^{\text{b}}/k_{\text{ip}})^{g}} = (1-v^{\text{b}}/k_{\text{ip}})(v^{\text{b}}/k_{\text{ip}})^{g} + O\left[(v^{\text{b}}/k_{\text{ip}})^{\Delta}\right], \quad g<\Delta \\
P_{\text{tp}}(g;v^{\text{b}}/k_{\text{tp}}) &= \frac{(v^{\text{b}}/k_{\text{tp}})^{g}}{\sum_{g=\Delta}^{\infty}(v^{\text{b}}/k_{\text{tp}})^{g}} = (1-v^{\text{b}}/k_{\text{tp}})(v^{\text{b}}/k_{\text{tp}})^{g-\Delta}, \qquad g\geq\Delta.
\end{aligned} \tag{8}$$

The above equations are valid when $(k_{\text{ip}}/k_{\text{tp}})^{\Delta}$ is large, which we refer to as the stable peloton regime (SPR). The condition for the SPR can intuitively be seen as combining the strength of the attraction between motors and roadblocks ($k_{\text{ip}}/k_{\text{tp}}$) and its range (Δ). Due to the SPR conditions exponential dependence on the roadblock shadow size, we expect physiological systems where the roadblock size is substantially larger than the motor step to always be in the SPR. In this limit, we have

$$P_{\mathrm{ip}}(g;v^{\mathrm{b}}/k_{\mathrm{ip}})=P_{\mathrm{TASEP}}(g;v^{\mathrm{b}}/k_{\mathrm{ip}}),\quad g<\Delta,\quad \text{and}\quad P_{\mathrm{tp}}(g;v^{\mathrm{b}}/k_{\mathrm{tp}})=P_{\mathrm{TASEP}}(g-\Delta;v^{\mathrm{b}}/k_{\mathrm{tp}}),\quad g\geq\Delta. \tag{9}$$

With these conditional distributions, we can now calculate the average gaps sizes for both regimes

$$\langle g\rangle_{\mathrm{ip}}^{\mathrm{b}}=\sum_{g=0}^{\infty}gP_{\mathrm{TASEP}}(g;v^{\mathrm{b}}/k_{\mathrm{ip}})=\frac{v^{\mathrm{b}}}{k_{\mathrm{ip}}-v^{\mathrm{b}}},\quad \langle g\rangle_{\mathrm{tp}}^{\mathrm{b}}=\sum_{g=\Delta}^{\infty}gP_{\mathrm{TASEP}}(g-\Delta;v^{\mathrm{b}}/k_{\mathrm{tp}})=\Delta+\frac{v^{\mathrm{b}}}{k_{\mathrm{tp}}-v^{\mathrm{b}}}, \tag{10}$$

Defining p^{b} as the probability of a gap in the bulk being a trans-peloton gap, we can write the average gap between motors as $\langle g\rangle^{\mathrm{b}}=(1-p^{\mathrm{b}})\langle g\rangle_{\mathrm{ip}}^{\mathrm{b}}+p^{\mathrm{b}}\langle g\rangle_{\mathrm{tp}}^{\mathrm{b}}$. Taking the average motor size into account, the average motor density is the inverse of the typical distance between the fronts of neighboring motors,

$$\rho_{\mathrm{m}}^{\mathrm{b}}=\frac{1}{\langle g\rangle^{\mathrm{b}}+\delta_{\mathrm{m}}}=\frac{1}{\left(1-p^{\mathrm{b}}\right)\langle g\rangle_{\mathrm{ip}}^{\mathrm{b}}+p^{\mathrm{b}}\langle g\rangle_{\mathrm{tp}}^{\mathrm{b}}+\delta_{\mathrm{m}}}. \tag{11}$$

The relative fraction of trans peloton gaps

Combining the intra- and trans-peloton distributions we can write the complete gap-size distribution of the hierarchical TASEP as

$$P_{\mathrm{hTASEP}}(g;v^{\mathrm{b}}/k_{\mathrm{ip}},v^{\mathrm{b}}/k_{\mathrm{tp}},\Delta)=\begin{cases}(1-p^{\mathrm{b}})P_{\mathrm{TASEP}}(g;v^{\mathrm{b}}/k_{\mathrm{ip}}), & g<\Delta\\ p^{\mathrm{b}}P_{\mathrm{TASEP}}(g-\Delta;v^{\mathrm{b}}/k_{\mathrm{tp}}), & g\geq\Delta\end{cases}. \tag{12}$$

In steady state, the probabilistic flow from intra- to trans-peloton gaps (a peloton is split in two) and from trans- to intra-peloton gaps (two pelotons merge) should balance. The motor ahead of a gap of size $\Delta-1$ hops with an average rate v and extends the gap to size Δ, inducing the mean-field probabilistic flow $v^{\mathrm{b}}P_{\mathrm{hTASEP}}(\Delta-1;v^{\mathrm{b}}/k_{\mathrm{ip}},v^{\mathrm{b}}/k_{\mathrm{tp}},\Delta)=v^{\mathrm{b}}(1-p^{\mathrm{b}})P_{\mathrm{TASEP}}(\Delta-1;v^{\mathrm{b}}/k_{\mathrm{ip}})$. In turn, a motor behind a gap of size Δ hops forward with an average rate k_{tp} and decreases the gap to size $\Delta-1$, inducing the probabilistic flow $k_{\mathrm{tp}}P_{\mathrm{hTASEP}}(\Delta;v^{\mathrm{b}}/k_{\mathrm{ip}},v^{\mathrm{b}}/k_{\mathrm{tp}},\Delta)=k_{\mathrm{tp}}p^{\mathrm{b}}P_{\mathrm{TASEP}}(0;v^{\mathrm{b}}/k_{\mathrm{tp}})$. In the steady state these two flows should balance, and equating these rates gives

$$p^{\mathrm{b}}=\frac{[\langle g\rangle_{\mathrm{tp}}^{\mathrm{b}}-\Delta]}{[\langle g\rangle_{\mathrm{tp}}^{\mathrm{b}}-\Delta]+\langle g\rangle_{\mathrm{ip}}^{\mathrm{b}}\left(\dfrac{k_{\mathrm{ip}}}{v^{\mathrm{b}}}\right)^{\Delta}}. \tag{13}$$

Taken together, **Equations (10), (11),** and **(13)** relate the average density in the system to the velocity and the microscopic model parameters. In **Figure 2 C** we compare the gap-size distribution resulting from our heuristic arguments (solid lines) with ones generated through simulations of the BRM (dots) at different motor densities. In (**Supplementary file 1**) we also discuss how our general heuristic solution relates to the existing mean-field solution of the BRM (Loan et al., 1998).

Observable bulk quantities

In addition to the motor density, there are other interesting observables that can be calculated if we know the average velocity in the bulk. Among them are the current of motors, $J=\rho_{\mathrm{m}}^{\mathrm{b}}v^{\mathrm{b}}$, and the average number of motors in a peloton, $\langle n_{\mathrm{p}}\rangle^{\mathrm{b}} = 1/p^{\mathrm{b}}$. Further, only gaps between pelotons are filled with roadblocks, and then typically only beyond the roadblock shadow. If we let $\rho_{\mathrm{rb}}^{\mathrm{eq}}$ be the equilibrium roadblock occupancy in the absence of motor activity, we can estimate the average roadblock occupancy as

$$\rho_{\mathrm{rb}}^{\mathrm{b}} = \rho_{\mathrm{rb}}^{\mathrm{eq}} \frac{p^{\mathrm{b}}[\langle g\rangle_{\mathrm{tp}}^{\mathrm{b}} - \Delta]}{\langle g\rangle^{\mathrm{b}} + \delta_{\mathrm{m}}}. \tag{14}$$

In **Figure 3** we plot the motor velocity, the current of motors, roadblock occupancy, and the average number of motors in a peloton as a function of the total density of motors on the track.

Asymptotic behavior in the SPR

We here show how **Equations (10), (11),** and **(13)** can be solved explicitly in terms of the motor density rather than velocity in the limit SPR. For notational convenience we introduce the average excess trans-peloton gap $\langle \tilde{g}\rangle_{\mathrm{tp}}^{\mathrm{b}}$ and the critical density ρ_0, to write **Equation (13)** as

$$p^{\mathrm{b}} = \frac{\langle \tilde{g}\rangle_{\mathrm{tp}}^{\mathrm{b}}\rho_0}{1+\langle \tilde{g}\rangle_{\mathrm{tp}}^{\mathrm{b}}\rho_0}, \quad \langle \tilde{g}\rangle_{\mathrm{tp}}^{\mathrm{b}} = \langle g\rangle_{\mathrm{tp}}^{\mathrm{b}} - \Delta = \frac{v^{\mathrm{b}}}{k_{\mathrm{tp}} - v^{\mathrm{b}}}, \quad \rho_0 = \frac{1}{\langle g\rangle_{\mathrm{ip}}^{\mathrm{b}}}\left(\frac{v^{\mathrm{b}}}{k_{\mathrm{ip}}}\right)^{\Delta}. \tag{15}$$

In the SPR, the transition density ρ_0 is very small by definition. In the limit $\rho_0\langle \tilde{g}\rangle_{\mathrm{tp}}^{\mathrm{b}} \gg 1$, pelotons are small and p^{b} is close to one, and **Equation (3)** can be written as

$$1/\rho_{\mathrm{m}}^{\mathrm{b}} - \delta_{\mathrm{m}} \approx \langle g\rangle_{\mathrm{ip}}^{\mathrm{b}} \tag{16}$$

Here we have a system controlled by the tpTASEP. In the limit $\rho_0\langle \tilde{g}\rangle_{\mathrm{tp}}^{\mathrm{b}} \ll 1$, pelotons are large, p^{b} is small, and **Equation (11)** can be written as

$$1/\rho_{\mathrm{m}}^{\mathrm{b}} - \delta_{\mathrm{m}} \approx \langle g\rangle_{\mathrm{ip}}^{\mathrm{b}} + \langle \tilde{g}\rangle_{\mathrm{tp}}^{\mathrm{b}}(\langle \tilde{g}\rangle_{\mathrm{tp}}^{\mathrm{b}} + \Delta)\rho_0. \tag{17}$$

If the first two terms on the right hand side dominate, we have the standard ipTASEP. If the last term dominates, we have a composite system. Taken together, there are three limits given by

$$\begin{aligned}
&\langle g\rangle_{\mathrm{tp}}^{\mathrm{b}} \approx 1/\rho_{\mathrm{m}}^{\mathrm{b}} - \delta_{\mathrm{m}}, && \rho_{\mathrm{m}}^{\mathrm{b}} \ll \rho_0 \\
&\langle \tilde{g}\rangle_{\mathrm{tp}}^{\mathrm{b}} \approx \frac{1}{\sqrt{\rho_0\rho_{\mathrm{m}}^{\mathrm{b}}}}, && \rho_0 \ll \rho_{\mathrm{m}}^{\mathrm{b}} \ll \rho_1 = \frac{1}{\langle g\rangle_{\mathrm{ip}}^{\mathrm{b}} + \delta_{\mathrm{m}}} \\
&\langle g\rangle_{\mathrm{ip}}^{\mathrm{b}} \approx 1/\rho_{\mathrm{m}}^{\mathrm{b}} - \delta_{\mathrm{m}}, && \rho_1 \ll \rho_{\mathrm{m}}^{\mathrm{b}}.
\end{aligned} \tag{18}$$

In the middle regime $\langle \tilde{g}\rangle_{\mathrm{tp}}^{\mathrm{b}}$ is large, and the average velocity (see **Equation (10)**) is close to k_{tp},

$$v^{\mathrm{b}} = k_{\mathrm{tp}}\left(1 - \sqrt{\rho_0\rho_{\mathrm{m}}^{\mathrm{b}}}\right). \tag{18}$$

Using **Equations (18)** and **(18),** all observables can be written to leading order in $1/\rho_0$ as

$$v^{\mathrm{b}} = k_{\mathrm{tp}}, \quad \langle g \rangle_{\mathrm{ip}}^{\mathrm{b}} = \frac{k_{\mathrm{tp}}}{k_{\mathrm{ip}} - k_{\mathrm{tp}}}, \quad \langle g \rangle_{\mathrm{tp}}^{\mathrm{b}} = \frac{1}{\sqrt{\rho_0 \rho_{\mathrm{m}}^{\mathrm{b}}}}, \quad \langle n_{\mathrm{p}} \rangle^{\mathrm{b}} = \sqrt{\frac{\rho_{\mathrm{m}}^{\mathrm{b}}}{\rho_0}}, \quad \frac{\rho_{\mathrm{rb}}^{\mathrm{b}}}{\rho_{\mathrm{rb}}^{\mathrm{eq}}} = 1 - \frac{\rho_{\mathrm{m}}^{\mathrm{b}}}{\rho_1}, \quad \rho_0 = \frac{k_{\mathrm{ip}} - k_{\mathrm{tp}}}{k_{\mathrm{tp}}} \left(\frac{k_{\mathrm{tp}}}{k_{\mathrm{ip}}} \right)^{k_{\mathrm{tp}}\tau + \delta_{\mathrm{rb}}} \tag{19}$$

In this regime, ($\rho_0 \ll \rho_{\mathrm{m}} \ll \rho_1$), the average bulk peloton size is large, and that is why we refer to this as the stable peloton regime.

Initiation limited dynamics

Without roadblocks, and if the initiation rate k_{in} is limiting, the density and the distribution of motors at the start of the lattice are the same as in the bulk (MacDonald et al., 1968). With the inclusion of roadblocks, the microscopic organization among motors and roadblocks can change from the start of the lattice to the bulk. Here we assume that the density of motors is low enough, such that once a motor is initiated it is only slowed down by other motors when it encounters a peloton. This condition means that once the initiation site is cleared, motors step away much faster at the beginning of the lattice than a new motor typically initiates. We will refer to this regime as the slow initiation regime, and we detail its extent below.

The formation of pelotons

A schematic kymograph for the TASEP with roadblocks and open boundary conditions is shown in **Figure 6**. At the start of the lattice, the time gaps between newly initiated motors are exponentially distributed with average time $1/k_{\mathrm{in}}$. As the motors move into the system, those motors that happened to have a roadblock bound ahead will start inducing peloton-forming traffic jams. For convenience we here call these jams proto-pelotons, and they will grow until all motors between roadblocks are absorbed into one peloton. Once all motors are collected into pelotons, we will refer to these as the fully formed pelotons. We here set out to determine the nature of this peloton formation, and what effects it has on both motor and roadblock density profiles.

In all the expressions below, the superscript ‘in’ refers to the first site after the initiation site for which $x = 0$. For a roadblock to bind to the first site after a motor just left, the motor first has to take δ_{rb} steps and then a roadblock has to bind, all before another motor initiates. Considering the splitting probabilities for each step, we can write the probability of a roadblock binding between two motor initiation events as

$$p^{\mathrm{in}} = \left(\frac{1}{1 + k_{\mathrm{in}} \tau_{\mathrm{m}}^{\mathrm{in}}} \right)^{\delta_{\mathrm{rb}}} \frac{1}{1 + k_{\mathrm{in}} \tau}. \tag{20}$$

Here $\tau_{\mathrm{m}}^{\mathrm{in}}$ is the average time it takes a motor to take a step at the start of the track,

$$\tau_{\mathrm{m}}^{\mathrm{in}} = \frac{1 - p^{\mathrm{in}}}{k_{\mathrm{ip}}} + \frac{p^{\mathrm{in}}}{k_{\mathrm{tp}}}. \tag{21}$$

The definition of the slow initiation regime implies $\tau_{\mathrm{m}}^{\mathrm{in}} \ll 1/k_{\mathrm{in}}$, and **Equation (20)** can be simplified as

$$p^{\mathrm{in}} = \frac{e^{-\delta_{\mathrm{rb}} \tau_{\mathrm{m}}^{\mathrm{in}} k_{\mathrm{in}}}}{1 + k_{\mathrm{in}} \tau}. \tag{22}$$

Equation (21) and **(22)** can be used to solve for p^{in} explicitly in the steady state,

$$p^{\mathrm{in}} = \Lambda^{-1} W\left(\frac{k_{\mathrm{in}}\tau}{1+k_{\mathrm{in}}\tau} \delta_{\mathrm{rb}} \Lambda e^{-k_{\mathrm{in}}\delta_{\mathrm{rb}}/k_{\mathrm{ip}}} \right), \quad \Lambda = \left(\frac{1}{k_{\mathrm{tp}}} - \frac{1}{k_{\mathrm{ip}}} \right) \frac{1}{\tau}, \tag{23}$$

where W is the Lambert W function. In the limit of low initiation rates we can write

$$p^{\mathrm{in}} = \frac{1}{1+k_{\mathrm{in}}\tilde{\tau}}, \quad \tilde{\tau} = \tau + \delta_{\mathrm{rb}} / k_{\mathrm{tp}}. \tag{24}$$

Next we calculate the typical time it takes for n_{p}^{*} motors to aggregate into a peloton. Let Δx be the typical distance that the proto-peloton back end moves between two motors joining (**Figure 6**). From the geometry of typical times and distances sketched in the kymograph of **Figure 6**, we can write

$$\left.\begin{aligned} &\Delta t\, k_{\mathrm{ip}} = \Delta x \\ &\langle g \rangle_{\mathrm{ip}}^{\mathrm{in}} = \frac{k_{\mathrm{tp}}}{k_{\mathrm{ip}} - k_{\mathrm{tp}}} \\ &\left(1/k_{\mathrm{in}} + \delta_{\mathrm{m}}/k_{\mathrm{ip}} + \Delta t\right) k_{\mathrm{tp}} = \Delta x + \delta_{\mathrm{m}} + \langle g \rangle_{\mathrm{ip}}^{\mathrm{in}} \end{aligned}\right\} \Rightarrow \Delta x = \frac{1}{k_{\mathrm{in}}\tau\Lambda} - \delta_{\mathrm{rb}}, \tag{25}$$

where Λ is given in **Equation (23).** In the last step above, we used the fact that we are considering the slow initiation regime, $k_{\mathrm{in}} \ll k_{\mathrm{ip}}, k_{\mathrm{tp}}$. Proto-pelotons grow as more and more motor catch up, and again ignoring correlations, the final size n_{p}^{*} of a proto peloton is geometrically distributed as

$$P(n_{\mathrm{p}}^{*}) = p^{\mathrm{in}}(1-p^{\mathrm{in}})^{n_{\mathrm{p}*}-1} \quad \Rightarrow \quad \langle n_{\mathrm{p}}^{*} \rangle = 1/p^{\mathrm{in}}. \tag{26}$$

Here the first factor in the probability function accounts for the probability of having a roadblock in a gap, and the following factors accounts for the probability of having no roadblocks in the preceding $n_{\mathrm{p}}^{*}-1$ gaps. The probability that a proto-peloton is still growing at position x, or equivalently the probability that $n_{\mathrm{p}}^{*} > x/\Delta x$, is then given by

$$P_{\mathrm{grow}}(x) = \sum_{n_{\mathrm{p}*} > x/\Delta x} p^{\mathrm{in}}(1-p^{\mathrm{in}})^{n_{\mathrm{p}}^{*}-1} = (1-p^{\mathrm{in}})^{x/\Delta x}. \tag{27}$$

Letting $\langle n_{\mathrm{p}}(x) \rangle$ be the size of the average proto-peloton at a distance x from the initiation site, we can now write down the discrete evolution equation $\langle n_{\mathrm{p}}(x+\Delta x) \rangle = \langle n_{\mathrm{p}}(x) \rangle + 1 \cdot P_{\mathrm{grow}}$, with $\langle n_{\mathrm{p}}(0) \rangle = 1$, giving

$$\langle n_{\mathrm{p}}(x) \rangle = \sum_{n=1}^{x/\Delta x} (1-p^{\mathrm{in}})^{n} + \langle n_{\mathrm{p}}(0) \rangle = \langle n_{\mathrm{p}}^{*} \rangle - \left[\langle n_{\mathrm{p}}^{*} \rangle - 1 \right] e^{-x/x^{*}}, \quad x^{*} = -\Delta x / \ln\left(1-p^{\mathrm{in}}\right). \tag{28}$$

Though strictly only true for x in multiples of Δx, we take the above equation to be valid for any position $x \geq 0$.

The macroscopic effects of peloton formation

We now turn to calculate how the gradual growth of the proto pelotons impacts the motor density and velocity. The motor number density $\rho_{\mathrm{m}}(x)$ at any position x is defined as the fraction of time that a site is occupied by (say) the front of a motor. The proto-peloton size at position x tells us that the fraction $\langle n_{\mathrm{p}}(x)\rangle p_{\mathrm{in}}$ motors take an average time $1/k_{\mathrm{tp}}$ to step, while the rest take $1/k_{\mathrm{ip}}$, giving the average stepping time

$$\tau_{\mathrm{m}}(x) = \frac{\langle n_{\mathrm{p}}(x)\rangle p^{\mathrm{in}}}{k_{\mathrm{tp}}} + \frac{1-\langle n_{\mathrm{p}}(x)\rangle p^{\mathrm{in}}}{k_{\mathrm{ip}}}, \quad \tau_{\mathrm{m}}(0) = \tau_{\mathrm{m}}^{\mathrm{in}}. \tag{29}$$

The total time T between the seeding of two pelotons (**Figure 6**) averages over peloton sizes to

$$\langle T\rangle = \langle n_{\mathrm{p}}^{*}\rangle \left(1/k_{\mathrm{in}} + \delta_{\mathrm{m}}\tau_{\mathrm{m}}^{\mathrm{in}}\right). \tag{30}$$

The fraction of time that the track is occupied by motors at position x is then

$$\rho_{\mathrm{m}}(x) = \frac{\langle n_{\mathrm{p}}^{*}\rangle \tau_{\mathrm{m}}(x)}{\langle T\rangle} = \frac{\tau_{\mathrm{m}}(x)}{1/k_{\mathrm{in}} + \delta_{\mathrm{m}}\tau_{\mathrm{m}}^{0}} = \rho_{\mathrm{m}}^{*} + (\rho_{\mathrm{m}}^{\mathrm{in}} - \rho_{\mathrm{m}}^{*})e^{-x/x^{*}}. \tag{36}$$

where the ρ_{m}^{*} denotes the motor density where the proto pelotons have fully formed. The average motor hopping rate can similarly be written as

$$k_{\mathrm{m}}(x) = p^{\mathrm{in}}\langle n_{\mathrm{p}}(x)\rangle k_{\mathrm{tp}} + (1-p^{\mathrm{in}}\langle n_{\mathrm{p}}(x)\rangle)k_{\mathrm{ip}} = k^{*} + (k^{\mathrm{in}} - k^{*})e^{-x/x^{*}}. \tag{31}$$

Though true for the TASEP, that here the average motor hopping rate (**Equation (31)**) is typically not the same as the average velocity $v(x) = \tau_{\mathrm{m}}^{-1}(x)$ in our system. With the velocity defined this way, it satisfies the standard relation $J = \rho_{\mathrm{m}}(x)v(x)$ where $J = \langle n_{\mathrm{p}}\rangle^{*}/\langle \mathrm{T}\rangle$ is the flux of motors.

In **Figure 6** we indicate the times and positions where there typically are roadblocks in pink. Moving away from the initiation site, the fraction of time a site is occupied by roadblocks grows because motors that have not yet caught up with a proto peloton move faster than the proto pelotons themselves. The moving front of equilibrating roadblocks (intersection of white and pink region in **Figure 6**) is typically offset with respect to the last motor of the peloton by a distance δ_{rb} (see dashed square in **Figure 6**). Taking the offset δ_{rb} into account, **Equation (27)** implies that a fraction $P_{\mathrm{grow}}(x+\delta_{\mathrm{rb}})$ of the proto pelotons is still evolving when the front of equilibrating roadblocks is at position x. The increase of the average time a site at position x (see **Figure 6**) is occupied by a roadblock then grows with distance as

$$t_{\mathrm{rb}}(x+\Delta x) = t_{\mathrm{rb}}(x) + \left(1/k_{\mathrm{tp}} - 1/k_{\mathrm{ip}}\right)\Delta x P_{\mathrm{grow}}(x+\delta_{\mathrm{rb}}), \quad t_{\mathrm{rb}}(0) = 1/k_{\mathrm{in}}. \tag{32}$$

This expression can be summed in the same manner as we previously summed to solve for $\langle n_{\mathrm{p}}(x)\rangle$ in **Equation (28),** yielding

$$t_{\mathrm{rb}}(x)=\left[1/k_{\mathrm{tp}}-1/k_{\mathrm{ip}}\right]\Delta x e^{-\delta_{\mathrm{rb}}/x^{*}}\left(\langle n_{\mathrm{p}}^{*}\rangle-1\right)\left(1-e^{-x/x^{*}}\right)+1/k_{\mathrm{in}}. \tag{33}$$

The total fraction of time a site is covered by roadblocks is now

$$\rho_{\mathrm{rb}}(x)=\rho_{\mathrm{rb}}^{\mathrm{eq}}\frac{t_{\mathrm{rb}}(x)}{\langle T\rangle}=\rho_{\mathrm{rb}}^{*}-(\rho_{\mathrm{rb}}^{\mathrm{in}}-\rho_{\mathrm{rb}}^{*})e^{-x/x^{*}}. \tag{34}$$

Relative changes are often easier to measure experimentally than absolute changes, therefore we here also give the relative changes in velocity and density at the beginning, and compared to well after the pelotons are formed

$$\frac{\rho_{\mathrm{m}}^{*}-\rho_{\mathrm{m}}^{\mathrm{in}}}{\rho_{\mathrm{m}}^{*}}=(1-p^{\mathrm{in}})\left(1-\frac{k_{\mathrm{tp}}}{k_{\mathrm{ip}}}\right),\quad \frac{v^{*}-v^{\mathrm{in}}}{v^{*}}=-(1-p^{\mathrm{in}})\left(\frac{k_{\mathrm{ip}}}{k_{\mathrm{tp}}}-1\right),\quad \frac{\rho_{\mathrm{rb}}^{*}-\rho_{\mathrm{rb}}^{\mathrm{in}}}{\rho_{\mathrm{rb}}^{*}}=\frac{1}{1+\frac{p^{\mathrm{in}}}{1-p^{\mathrm{in}}}\frac{\Delta x+\delta_{\mathrm{m}}}{\Delta x}\cdot e^{\delta_{\mathrm{rb}}/x^{*}}}. \tag{35}$$

To have an appreciable motor density and velocity evolution, we need only the typical peloton to have a size of a few motors. In the limit of low initiation rates, the above can be written as

$$\frac{\rho_{\mathrm{m}}^{*}-\rho_{\mathrm{m}}^{\mathrm{in}}}{\rho_{\mathrm{m}}^{*}}=\frac{k_{\mathrm{in}}\tilde{\tau}}{1+k_{\mathrm{in}}\tilde{\tau}}\left(1-\frac{k_{\mathrm{tp}}}{k_{\mathrm{ip}}}\right),\quad \frac{v^{*}-v^{\mathrm{in}}}{v^{*}}=-\frac{k_{\mathrm{in}}\tilde{\tau}}{1+k_{\mathrm{in}}\tilde{\tau}}\left(\frac{k_{\mathrm{ip}}}{k_{\mathrm{tp}}}-1\right),\quad \frac{\rho_{\mathrm{rb}}^{*}-\rho_{\mathrm{rb}}^{\mathrm{in}}}{\rho_{\mathrm{rb}}^{*}}=\frac{k_{\mathrm{in}}\tilde{\tau}}{e^{\delta_{\mathrm{rb}}/x^{*}}+k_{\mathrm{in}}\tilde{\tau}}. \tag{35}$$

Bursts from terminating pelotons

The peloton-forming dynamics of our model will manifest as burst of motor activity if viewed from a specific position (for example the transcription-termination site). Using the average velocity of the system, we can translate the average gap-sizes to average time gaps between motors arrivals

$$\tau_{\mathrm{ip}}=\frac{\langle g\rangle_{\mathrm{ip}}+\delta_{\mathrm{m}}}{v},\quad \tau_{\mathrm{tp}}=\frac{\langle g\rangle_{\mathrm{tp}}+\delta_{\mathrm{m}}}{v}. \tag{36}$$

Letting k_{tr} be the rate of reaction when the process is in the on state, k_{off} be the rate at which the system transitions to the off state, and k_{on} be the rate at which the system transitions back to the on state, we can relate our first-principles model to the phenomenological two-state model traditionally used to describe transcriptional bursts (**Figure 4 E**) (Thattai and Oudenaarden, 2001). As both models generate double exponentials, we relate them to each other by equating the time constant and the corresponding relative probabilistic weight. Since we are interested in describing transcriptional bursts, we here consider the limit where the two-state model gives clearly separated bursts, $k_{\mathrm{on}}\ll k_{\mathrm{off}}+k_{\mathrm{tr}}$. In this limit we have, to leading order in k_{on},

$$p=\frac{k_{\mathrm{off}}}{k_{\mathrm{off}}+k_{\mathrm{tr}}},\quad \tau_{\mathrm{ip}}=\frac{1}{k_{\mathrm{off}}+k_{\mathrm{tr}}},\quad \text{and}\quad \tau_{\mathrm{tp}}=\frac{1}{k_{\mathrm{on}}}\left(1+\frac{k_{\mathrm{off}}}{k_{\mathrm{tr}}}\right). \tag{37}$$

The relations in **Equation (37)** can be inverted to give

$$k_{\mathrm{tr}}=\frac{1-p}{\tau_{\mathrm{ip}}},\quad k_{\mathrm{off}}=\frac{p}{\tau_{\mathrm{ip}}},\quad \text{and}\quad k_{\mathrm{on}}=\frac{1}{(1-p)\tau_{\mathrm{tp}}}. \tag{38}$$

For the bulk we can in principle calculate the corresponding two-state model using **Equation (10)**, though this state is likely never reached. The physiologically more interesting situation is just after the initial pelotons have fully formed. The relative probability of a gap being between pelotons is then (see **Equation (24)**)

$$p = p^{\mathrm{in}} = \frac{1}{1 + k_{\mathrm{in}} \tilde{\tau}}. \tag{39}$$

Once the initial pelotons have formed beyond x^*, we know that the average velocity is k_{tp}, and we have

$$\langle g \rangle_{\mathrm{ip}}^{*} = \frac{k_{\mathrm{tp}}}{k_{\mathrm{ip}} - k_{\mathrm{tp}}} \quad \Rightarrow \quad \tau_{\mathrm{ip}}^{*} = \frac{1}{k_{\mathrm{ip}} - k_{\mathrm{tp}}} + \frac{\delta_{\mathrm{m}}}{k_{\mathrm{tp}}}. \tag{40}$$

The trans-peloton gaps can be written as (see **Figure 6**)

$$\langle T \rangle = \tau_{\mathrm{tp}}^{*} + \tau_{\mathrm{ip}}^{*}\left(\langle n_{\mathrm{p}} \rangle^{*} - 1 \right) \quad \Rightarrow \quad \tau_{\mathrm{tp}}^{*} = \langle T \rangle - \tau_{\mathrm{ip}}^{*} k_{\mathrm{in}} \tilde{\tau} = \left(\frac{1}{k_{\mathrm{in}}} + \frac{\delta_{\mathrm{m}}}{k_{\mathrm{tp}}} \right) + \left(\frac{1}{k_{\mathrm{in}}} - \frac{1}{k_{\mathrm{ip}} - k_{\mathrm{tp}}} \right) k_{\mathrm{in}} \tilde{\tau} \tag{41}$$

Combining **Equations (38)-(41)** we have

$$k_{\mathrm{tr}} = \frac{k_{\mathrm{in}} \tilde{\tau}}{1 + k_{\mathrm{in}} \tilde{\tau}} \frac{1}{\tau_{\mathrm{ip}}^{*}}, \quad k_{\mathrm{off}} = \frac{1}{1 + k_{\mathrm{in}} \tilde{\tau}} \frac{1}{\tau_{\mathrm{ip}}^{*}}, \quad \text{and} \quad k_{\mathrm{on}} = \frac{1 + k_{\mathrm{in}} \tilde{\tau}}{k_{\mathrm{in}} \tilde{\tau}} \frac{1}{\tau_{\mathrm{tp}}^{*}}. \tag{41}$$

In the main text we are interested in the case where motors are large and the initiation rate is low compared to motor stepping rates. In this limit we have

$$k_{\mathrm{tr}} = \frac{k_{\mathrm{in}} \tilde{\tau}}{1 + k_{\mathrm{in}} \tilde{\tau}} \frac{k_{\mathrm{tp}}}{\delta_{\mathrm{m}}}, \quad k_{\mathrm{off}} = \frac{1}{1 + k_{\mathrm{in}} \tilde{\tau}} \frac{k_{\mathrm{tp}}}{\delta_{\mathrm{m}}}, \quad \text{and} \quad k_{\mathrm{on}} = \frac{1}{\tilde{\tau} + \dfrac{k_{\mathrm{in}} \tilde{\tau}}{1 + k_{\mathrm{in}} \tilde{\tau}} \dfrac{\delta_{\mathrm{m}}}{k_{\mathrm{tp}}}} \approx \frac{1}{\tilde{\tau}}. \tag{42}$$

Here the approximate relation should be valid in the case of transcription through nucleosomes as here the roadblock are substantially larger than the motors, and $\tilde{\tau}$ is consequently substantially larger than $\delta_{\mathrm{m}} / k_{\mathrm{tp}}$.

The bulk state is never reached

With the parameter values in **Table 1**, the bulk state is given by

$$\langle g \rangle_{\mathrm{ip}}^{\mathrm{b}} \approx 0.4, \quad \langle g \rangle_{\mathrm{tp}}^{\mathrm{b}} \approx \frac{5 \cdot 10^{82}}{\sqrt{\rho_{\mathrm{m}}}}, \quad v^{\mathrm{b}} \approx 3/\mathrm{s}, \quad \langle n_{\mathrm{p}} \rangle^{\mathrm{b}} \approx 5 \cdot 10^{82} \sqrt{\rho_{\mathrm{m}}}. \tag{43}$$

From the above it is clear that the average steady-state peloton size $\langle n_{\mathrm{p}} \rangle^{\mathrm{b}}$ is in general enormous throughout the experimentally accessible range, and that the true bulk-dynamics will never be reached over a finite gene. Judging by the size of bulk pelotons, polymerases that meet along the gene stay together until termination—invariably producing bursts of RNA production.

Monte Carlo Simulations

We validate our heuristic arguments using a random-sequential-update Monte Carlo scheme with fixed time step dt to simulate our model. During a Monte Carlo step on a lattice of size $L+1$ there are $L+1$ possible events: all the motors on the lattice can make a step forward, bound roadblocks can unbind, roadblocks in solution can bind to an empty lattice site, and a motor can bind at the start of the lattice. The time step is chosen small enough that the probability of any event occurring with rate k in a time dt can be approximated as kdt. In our simulation k_{ip} is the fastest rate, and we choose $k_{\mathrm{ip}}dt = 0.1$. We verified that our results are robust towards changes in dt. Without roadblocks, the time to equilibration scales with the system size as $L^{3/2}$ [19]. With roadblocks, the time to equilibration is expected to be larger due to the slow peloton dynamics.

For the simulations with periodic boundary conditions we waited L^2/dt iterations for the system to reach steady state and let simulations run a total amount of $10L^2/dt$ iterations, and checked that the peloton size did not change for longer equilibration times. The velocities presented in **Figure 3** and **5** are calculated by averaging over the instantaneous hopping rates of the motors.

Acknowledgements

We thank Joachim Griesenbeck for insightful discussions, Misha Klein, Orkide Ordu, Behrouz Eslami, John van Noort and Stephan Grill for comments on the manuscript, and Ruben van Drongelen for help with questions about programming. MD and AAvdB acknowledge financial support from a TU Delft startup grant to MD. AAvdB further acknowledges financial support by the Netherlands Organization for Scientific Research (NWO/OCW), as part of the Frontiers of Nanoscience program.

Author contributions

MD and AAvdB designed research, performed the research, and wrote the paper. AAvdB performed the Monte Carlo simulations and analyzed the simulation data.

References

Albert, B., Léger-Silvestre, I., Normand, C., Ostermaier, M.K., Pérez-Fernández, J., Panov, K.I., Zomerdijk, J.C.B.M., Schultz, P., and Gadal, O. (2011). RNA polymerase I-specific subunits promote polymerase clustering to enhance the rRNA gene transcription cycle. J. Cell Biol. *192*, 277–293.

Angelov, D., Bondarenko, V. a, Almagro, S., Menoni, H., Mongélard, F., Hans, F., Mietton, F., Studitsky, V.M., Hamiche, A., Dimitrov, S., et al. (2006). Nucleolin is a histone chaperone with FACT-like activity and assists remodeling of nucleosomes. EMBO J. *25*, 1669–1679.

Belotserkovskaya, R., Oh, S., Bondarenko, V. a, Orphanides, G., Studitsky, V.M., and Reinberg, D. (2003). FACT facilitates transcription-dependent nucleosome alteration. Science *301*, 1090–1093.

Bintu, L., Ishibashi, T., Dangkulwanich, M., Wu, Y.-Y., Lubkowska, L., Kashlev, M., and Bustamante, C. (2012). Nucleosomal elements that control the topography of the barrier to transcription. Cell *151*, 738–749.

Blythe, R.A., and Evans, M.R. (2007). Nonequilibrium steady states of matrix-product form: a solver's guide. J. Phys. A Math. Theor. *40*, R333–R441.

Brogaard, K., Xi, L., Wang, J.-P., and Widom, J. (2012). A map of nucleosome positions in yeast at base-pair resolution. Nature *486*, 496–501.

Chong, S., Chen, C., Ge, H., and Xie, X.S. (2014). Mechanism of Transcriptional Bursting in Bacteria. Cell *158*, 314–326.

Chowdhury, D., Schadschneider, A., and Nishinari, K. (2005). Physics of transport and traffic phenomena in biology: From molecular motors and cells to organisms. Phys. Life Rev. *2*, 318–352.

Chubb, J.R., Trcek, T., Shenoy, S.M., and Singer, R.H. (2006). Transcriptional Pulsing of a Developmental Gene. Curr. Biol. *16*, 1018–1025.

Cole, H.A., Ocampo, J., Iben, J.R., Chereji, R. V, and Clark, D.J. (2014). Heavy transcription of yeast genes correlates with differential loss of histone H2B relative to H4 and queued RNA polymerases. Nucleic Acids Res. *42*, 12512–12522.

Cooper, G.M. (2000). Regulation of Transcription in Eukaryotes. In The Cell: A Molecular Approach. 2nd Edition, (Sinauer Associates),.

Core, L.J., Waterfall, J., and Lis, J.T. (2008). Nascent RNA Sequencing Reveals Widespread Pausing and Divergent Initiation at Human Promoters. Science *322*, 1845–1848.

Crick, F. (1970). Central Dogma of Molecular Biology. Nature *227*, 561–563.

Danko, C.G., Hah, N., Luo, X., Martins, A.L., Core, L., Lis, J.T., Siepel, A., and Kraus, W.L. (2013). Signaling Pathways Differentially Affect RNA Polymerase II Initiation, Pausing, and Elongation Rate in Cells. Mol. Cell *50*, 212–222.

Darzacq, X., Shav-Tal, Y., de Turris, V., Brody, Y., Shenoy, S.M., Phair, R.D., and Singer, R.H. (2007). In vivo dynamics of RNA polymerase II transcription. Nat. Struct. Mol. Biol. *14*, 796–806.

Dennis, P.P., Ehrenberg, M., Fange, D., and Bremer, H. (2009). Varying rate of RNA chain elongation during rrn transcription in Escherichia coli. J. Bacteriol. *191*, 3740–3746.

Derrida, B., Evans, M.R., Hakim, V., and Pasquier, V. (1993). Exact solution of a 1D asymmetric exclusion model using a matrix formulation. J. Phys. A Math. Gen. *26*, 1493–1517.

Dion, M.F., Kaplan, T., Kim, M., Buratowski, S., Friedman, N., and Rando, O.J. (2007). Dynamics of Replication-Independent Histone Turnover in Budding Yeast. Science *315*, 1405–1409.

Dobrzynski, M., and Bruggeman, F.J. (2009). Elongation dynamics shape bursty transcription. PNAS *106*, 2583–2588.

Finkelstein, I.J., and Greene, E.C. (2013). Molecular traffic jams on DNA. Annu. Rev. Biophys. *42*, 241–263.

Golding, I., Paulsson, J., Zawilski, S.M., and Cox, E.C. (2005). Real-time kinetics of gene activity in individual bacteria. Cell *123*, 1025–1036.

Goodsell, D.S. (2009). The Machinery of Life (Springer Sciences & Business Media).

Greive, S.J., and Hippel, P.H. Von (2005). Thinking quantitatively about transcriptional regulation. Nat. Rev. Mol. Cell Biol. *6*, 221–232.

Harper, F., and Puvion-Dutilleul, F. (1979). Non-Nucleolar Transcription Complexes of Rat Liver as Revealed by Spreading Isolated Nuclei. J Cell Sci *40*, 181–192.

Von Heijne, G., Nilsson, L., and Blomberg, C. (1977). Translation and messenger RNA secondary structure. J. Theor. Biol. *68*, 321–329.

Hodges, C., Bintu, L., Lubkowska, L., Kashlev, M., and Bustamante, C. (2009). Nucleosomal fluctuations govern the transcription dynamics of RNA polymerase II. Science *325*, 626–628.

Howard, J. (2001). Mechanics of Motor Proteins and the Cytoskeleton (Sunderland, Massachusetts: Sinauer Associates).

Hoyt, M.A., Hyman, A.A., and Bähler, M. (1997). Motor proteins of the eukaryotic cytoskeleton. Proc. Natl. Acad. Sci. U. S. A. *94*, 12747–12748.

Jamai, A., Imoberdorf, R.M., and Strubin, M. (2007). Continuous Histone H2B and Transcription-Dependent Histone H3 Exchange in Yeast Cells outside of Replication. Mol. Cell *25*, 345–355.

Jin, J., Bai, L., Johnson, D.S., Fulbright, R.M., Kireeva, M.L., Kashlev, M., and Wang, M.D. (2010). Synergistic action of RNA polymerases in overcoming the nucleosomal barrier. Nat. Struct. Mol. Biol. *17*, 745–752.

Jonkers, I., and Lis, J.T. (2015). Getting up to speed with transcription elongation by RNA polymerase II. Nat. Rev. Mol. Cell Biol. *16*, 167–177.

Kaern, M., Elston, T.C., Blake, W.J., and Collins, J.J. (2005). Stochasticity in gene expression: from theories to phenotypes. Nat. Rev. Genet. *6*, 451–464.

Kireeva, M.L., Walter, W., Tchernajenko, V., Bondarenko, V., Kashlev, M., and Studitsky, V.M. (2002). Nucleosome remodeling induced by RNA polymerase II: Loss of the H2A/H2B dimer during transcription. Mol. Cell *9*, 541–552.

Klumpp, S. (2011). Pausing and Backtracking in Transcription Under Dense Traffic Conditions. J. Stat. Phys. *142*, 1252–1267.

Klumpp, S., and Hwa, T. (2008). Stochasticity and traffic jams in the transcription of ribosomal RNA: Intriguing role of termination and antitermination. Proc. Natl. Acad. Sci. U. S. A. *105*, 18159–18164.

Kristjuhan, A., and Svejstrup, J.Q. (2004). Evidence for distinct mechanisms facilitating transcript elongation through chromatin in vivo. EMBO J. *23*, 4243–4252.

Kulaeva, O.I., Hsieh, F.-K., and Studitsky, V.M. (2010). RNA polymerase complexes cooperate to relieve the nucleosomal barrier and evict histones. Proc. Natl. Acad. Sci. U. S. A. *107*, 11325–11330.

Kunwar, A., John, A., Nishinari, K., Schadschneider, A., and Chowdhury, D. (2004). Collective traffic-like movement of ants on a trail: dynamical phases and phase transitions. J. Phys. Soc. Japan *73*, 2979–2985.

Laird, C.D., and Chooi, W.Y. (1976). Morphology of transcription units in Drosophila melanogaster. Chromosoma *58*, 193–218.

Lee, C.-K., Shibata, Y., Rao, B., Strahl, B.D., and Lieb, J.D. (2004). Evidence for nucleosome depletion at active regulatory regions genome-wide. Nat. Genet. *36*, 900–905.

Lee, W., Tillo, D., Bray, N., Morse, R.H., Davis, R.W., Hughes, T.R., and Nislow, C. (2007). A high-resolution atlas of nucleosome occupancy in yeast. Nat. Genet. *39*, 1235–1244.

Li, G., Xie, X.S., and Hirschfeld, T. (2011). Central dogma at the single-molecule level in living cells. Nature *475*, 308–315.

Liu, L.F., and Wang, J.C. (1987). Supercoiling of the DNA template during transcription. Proc. Natl. Acad. Sci. *84*, 7024–7027.

Loan, O.J.O., Evans, M.R., and Cates, M.E. (1998). Jamming transition in a homogeneous one-dimensional system : The bus route model. Phys. Rev. E *58*, 1404–1418.

van Loenhout, M.T.J., de Grunt, M. V, and Dekker, C. (2012). Dynamics of DNA Supercoils. Science *338*, 94–97.

Luger, K., Mäder, a W., Richmond, R.K., Sargent, D.F., and Richmond, T.J. (1997). Crystal structure of the nucleosome core particle at 2.8 A resolution. Nature *389*, 251–260.

Luijsterburg, M.S., White, M.F., van Driel, R., and Dame, R.T. (2008). The Major Architects of Chromatin: Architectural Proteins in Bacteria, Archaea and Eukaryotes. Crit. Rev. Biochem. Mol. Biol. *43*, 393–418.

MacDonald, C.T., Gibbs, J.H., and Pipkin, A.C. (1968). Kinetics of Biopolymerization on Nucleic Acid Templates. Biopolymers *6*, 1–25.

Mao, Y., Liu, H., Liu, Y., and Tao, S. (2014). Deciphering the rules by which dynamics of mRNA secondary structure affect translation efficiency in Saccharomyces cerevisiae. Nucleic Acids Res. *42*, 4813–4822.

Mazurkiewicz, J., Kepert, J.F., and Rippe, K. (2006). On the mechanism of nucleosome assembly by histone chaperone NAP1. J. Biol. Chem. *281*, 16462–16472.

Mcknight, S.L., and Miller, O.L. (1979). Post-replicative D . melanogaster Nonribosomal Embryos Transcription Units in. Cell *17*, 551–563.

Murthy, K.P.N., and Schutz, G.M. (1998). Aging in two- and three-particle annihilation processes. Phys. Rev. E *57*, 1388–1394.

Parmeggiani, A., Franosch, T., and Frey, E. (2004). Totally asymmetric simple exclusion process with Langmuir kinetics. Phys. Rev. E *70*, 046101.

Pelechano, V., Chavez, S., and Perez-Ortin, J.E. (2010). A Complete Set of Nascent Transcription Rates for Yeast Genes. PLoS One *5*, e15442.

Raj, A., and van Oudenaarden, A. (2008). Nature, nurture, or chance: stochastic gene expression and its consequences. Cell *135*, 216–226.

Raj, A., Peskin, C.S., Tranchina, D., Vargas, D.Y., and Tyagi, S. (2006). Stochastic mRNA Synthesis in Mammalian Cells. *4*.

Rufiange, A., Jacques, P. ??tienne, Bhat, W., Robert, F., and Nourani, A. (2007). Genome-Wide Replication-Independent Histone H3 Exchange Occurs Predominantly at Promoters and Implicates H3 K56 Acetylation and Asf1. Mol. Cell *27*, 393–405.

Schadschneider, A., Chowdhury, D., and Nishinari, K. (2011). Stochastic Transport in Complex Systems (Elsevier B.V.).

Schwabish, M. a, and Struhl, K. (2004). Evidence for eviction and rapid deposition of histones upon transcriptional elongation by RNA polymerase II. Mol. Cell. Biol. *24*, 10111–10117.

Shaevitz, J.W., Abbondanzieri, E. a, Landick, R., and Block, S.M. (2003). Backtracking by single RNA polymerase molecules observed at near-base-pair resolution. Nature *426*, 684–687.

Shivaswamy, S., Bhinge, A., Zhao, Y., Jones, S., Hirst, M., and Iyer, V.R. (2008). Dynamic remodeling of individual nucleosomes across a eukaryotic genome in response to transcriptional perturbation. PLoS Biol. *6*, 0618–0630.

So, L.-H., Ghosh, A., Zong, C., Sepúlveda, L. a, Segev, R., and Golding, I. (2011). General properties of transcriptional time series in Escherichia coli. Nat. Genet. *43*, 554–560.

Tantale, K., Mueller, F., Kozulic-Pirher, A., Lesne, A., Victor, J.-M., Robert, M.-C., Capozi, S., Chouaib, R., Bäcker, V., Mateos-Langerak, J., et al. (2016). A single-molecule view of transcription reveals convoys of RNA polymerases and multi-scale bursting. Nat. Commun. *7*, 12248.

Thattai, M., and Oudenaarden, A. Van (2001). Intrinsic noise in gene regulatory networks. PNAS *98*, 8614–8619.

Thiriet, C., and Hayes, J.J. (2005). Replication-independent core histone dynamics at transcriptionally active loci in vivo. Genes Dev. *19*, 677–682.

Trenchard, H. (2015). The peloton superorganism and protocooperative behavior. Appl. Math. Comput. *270*, 179–192.

Voliotis, M., Cohen, N., Molina-París, C., and Liverpool, T.B. (2008). Fluctuations, pauses, and backtracking in DNA transcription. Biophys. J. *94*, 334–348.

Weiner, A., Hughes, A., Yassour, M., Rando, O.J., and Friedman, N. (2010). High-Resolution Nucleosome Mapping Reveals Transcription-Dependent Promoter Packaging. Genome Res. 90–100.

Worcel, A., Han, S., and Wong, M.L. (1978). Assembly of newly replicated chromatin. Cell *15*, 969–977.

Yuan, G.-C. (2005). Genome-Scale Identification of Nucleosome Positions in S. cerevisiae. Science *309*, 626–630.

Zenklusen, D., Larson, D.R., and Singer, R.H. (2008). Single-RNA counting reveals alternative modes of gene expression in yeast. TL - 15. Nat. Struct. Mol. Biol. *15 VN - r*, 1263–1271.

Figures

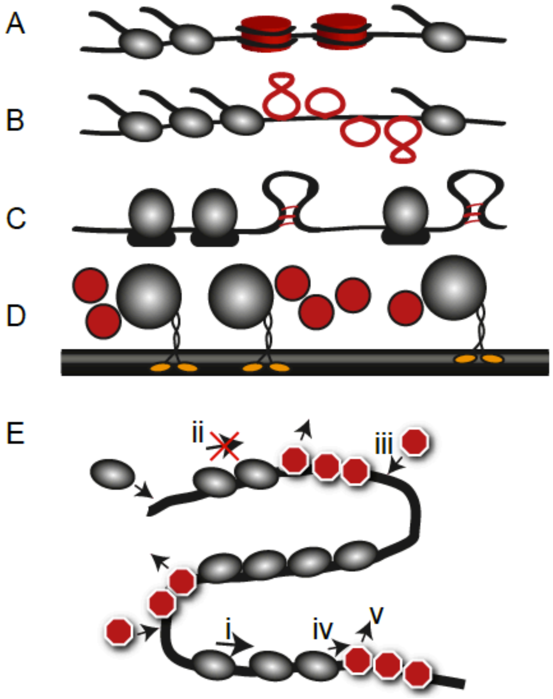

Figure 1: Examples of systems described by our model. A) RNAP interacting with nucleosomes or other DNA binding proteins (the example explicitly considered in this paper). **B)** RNAP interacting with supercoils. The buildup of positive supercoils ahead of a polymerase (Liu and Wang, 1987) can substantially slow down the motion of a polymerase (Chong et al., 2014). For a polymerase following closely behind another polymerase this effect does not occur, as negative supercoils generated behind the leading polymerase cancel the positive supercoils generated by the trailing polymerase. **C)** Ribosomes interacting with secondary RNA structures that act as dynamic roadblocks (Von Heijne et al., 1977; Mao et al., 2014). **D)** Kinesin transporting cargo along microtubules through the visco-elastic cellular interior of the cell (here presented as red dots). As a cargo passes, the surrounding material is pushed out of the way, and relaxes back over a finite timescale. The finite relaxation time could allow closely trailing cargos to move with less resistance, generating a dynamic attraction. **E)** Schematic illustration of model features i)-v) (see text) for motors (ovals) interacting with dynamic roadblocks (octagons) along a one-dimensional track.

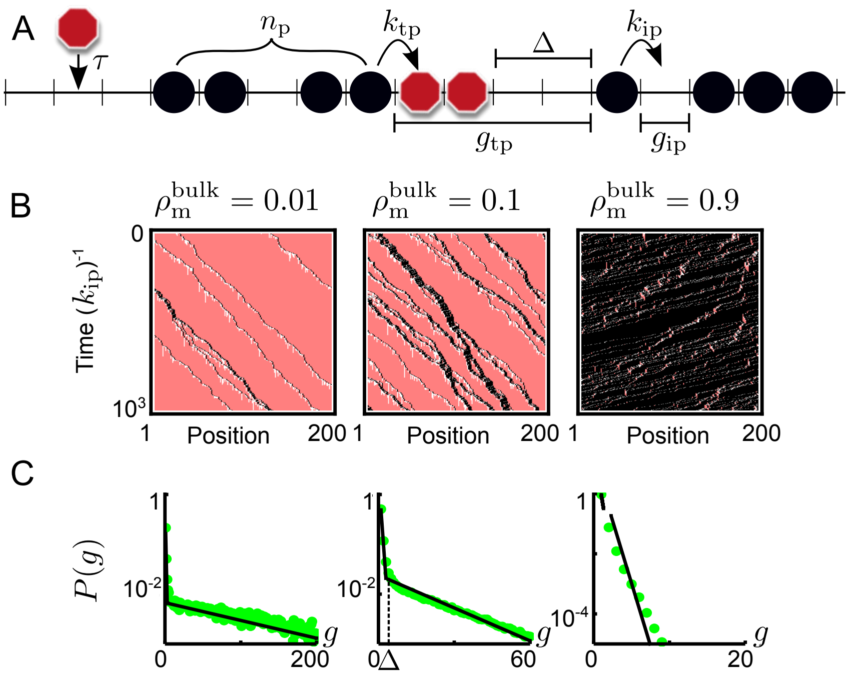

Figure 2: The hierarchy of TASEPs and its limiting behaviors. A) Schematic illustration of the rules of the BRM. Microscopic rates are indicated, as well are the roadblock-DNA binding equilibration time τ, the roadblock shadow Δ, instances of the peloton size $n_{\rm p}$, and the gap size for both trans- and intra-peloton gaps, $g_{\rm ip}$ and $g_{\rm tp}$ respectively. **B)** Kymographs generated through Monte-Carlo simulations of the BRM for systems (supplementary file **Figure2-sourcedata1**) with low roadblock density (left), intermediate roadblock density (middle), and high roadblock densities (right) for $k_{\rm ip}\tau = 10$. Motors are shown in black, roadblocks in pink and the roadblock shadow is visible as a roadblock depleted region (white) behind the motors. **C)** The gap-size distributions (green dots) corresponding to B) (supplementary file **Figure2-sourcedata2**), together with our analytical results (black lines). The left and right panel show a dominating single exponential (note the log-scales on the y-axes), which corresponds to a single TASEP, while the gap size distribution in the middle panel shows two exponentials, which suggests that the system can be described as a hierarchical combination of two TASEPs.

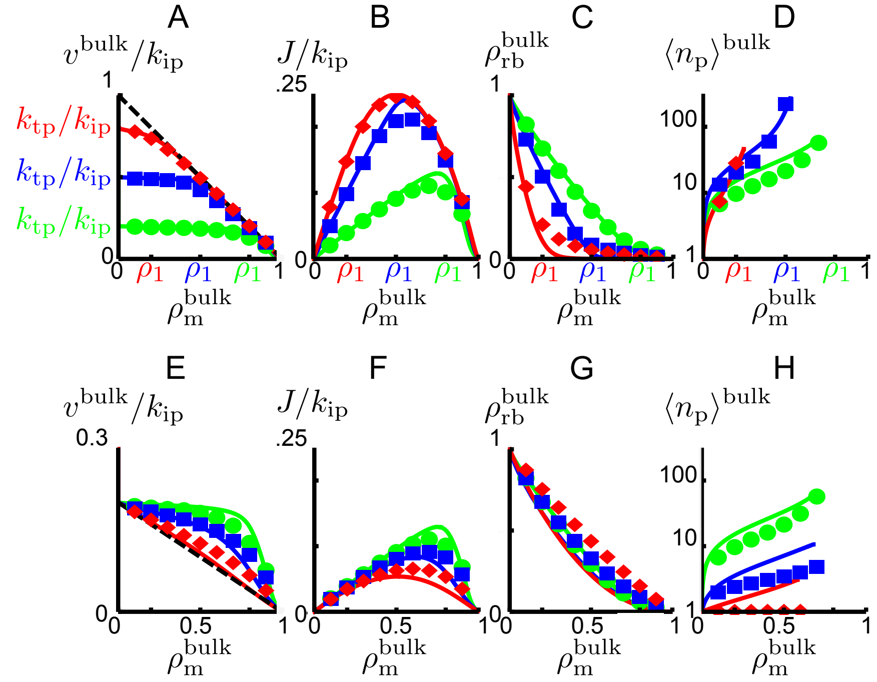

Figure 3: General model captures bulk dynamics of the BRM. Solid lines are analytical predictions and symbols are results from Monte Carlo simulations (supplementary file **Figure3-sourcedata1**). Within the rows, each color represents the same parameter values**,** while green represents the same parameter values across all panels. **A-D)** Systems in to the SPR: the parameter values are $k_{\rm ip}\tau = 20$ for all curves, with $k_{\rm tp}/k_{\rm ip} = 0.8$ (red), $k_{\rm tp}/k_{\rm ip} = 0.5$ (blue), and $k_{\rm tp}/k_{\rm ip} = 0.2$ (green). The dashed line in A) is the velocity relation for the ipTASEP. **E-H)** Sweep from stable to non-stable pelotons: the parameter values are $k_{\rm tp}/k_{\rm ip} = 0.2$ for all curves, and $k_{\rm ip}\tau = 20$ (green), $k_{\rm ip}\tau = 10$ (blue), $k_{\rm ip}\tau = 2$ (red). The dashed line in E) is the velocity relation for the tpTASEP. In A) and E) we show the velocity, in B) and F) the motor current, in C) and G) the roadblock occupancy and in D) and H) the peloton size, all as a function of motor density. In the SPR, it only makes sense to talk about pelotons when there are roadblocks in the system ($\rho_{\rm m}^{\rm bulk} < \rho_1$), and we only show the burst size as a function of motor activity for these densities. For small enough roadblock shadows (red and blue line in Figure E-H) our description breaks down as the system falls outside the SPR.

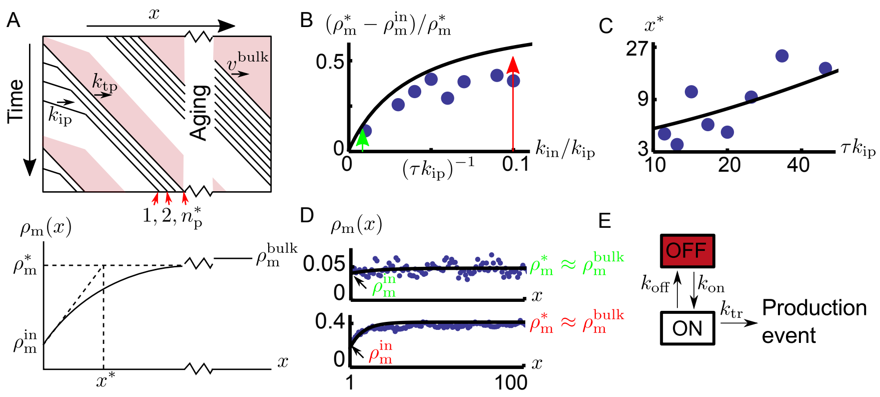

Figure 4: Open boundary conditions in the SPR. A) A schematic kymograph showing motors (black lines) initially not interacting with each other, until they reach the growing peloton. Motors initiate from the left and then travel into the system, moving through roadblock depleted regions (white) and roadblock filled regions (pink). If a roadblock is deposited between two motor initiation events, the last motor propagates with rate $k_{\rm tp}$ and otherwise with rate $k_{\rm ip}$. After a typical distance x^*, a peloton of size $n_{\rm p}^*$ is formed. Below the kymograph we sketch the corresponding motor density. **B)** The dots are values for the relative change in motor density from the start of the lattice to the point where all the initial pelotons have formed, obtained by fitting an exponential distribution to the peloton forming region (estimated as the first $4x^*$ lattice points) of simulated data (supplementary file **Figure4-sourcedata1**). The line represents our theoretical predictions and the green and red arrows indicate the initiation rates used for **Figure D**. **C)** The distance x^* over which pelotons form as a function of the roadblock equilibration time for $k_{\rm in} = 0.1k_{\rm ip}$. The dots are values for x^* obtained by fitting an exponential distribution to the peloton forming region (estimated as the first $4x^*$ lattice points) of simulated data (supplementary file **Figure4-sourcedata1**), while the line represents our theoretical predictions. **D)** Motor density profiles for $\left(\tilde{\tau}k_{\rm ip}\right)^{-1} = 0.05$, and $k_{\rm in} = 0.01k_{\rm ip} < \left(\tilde{\tau}k_{\rm ip}\right)^{-1}$ in the top panel, and $k_{\rm in} = 0.1k_{\rm ip} > \left(\tilde{\tau}k_{\rm ip}\right)^{-1}$ for the lower panel. Blue dots are the result of Monte Carlo simulations and black lines are our analytical predictions. Note, there are no free parameters in any of the analytical predictions in B)-D). **E)** The phenomenological two-state model normally used to describe bursty transcription. In **Equation (4)** we report the parameters that would result from fitting the bursts generated by our model to the two-state model .

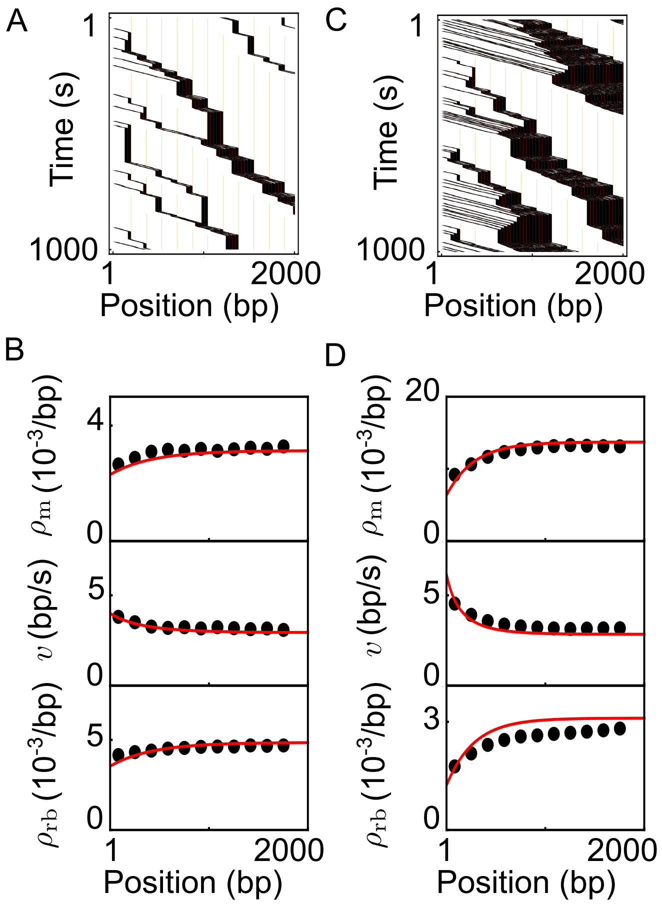

Figure 5: Predictions for RNAP II transcription on inducible genes in eukaryotes. The parameter values used are shown in **Table 1. A)** Kymograph for relatively moderate initiation rates. An RNAP II evicts a nucleosome when it passes its center (the dyads, indicated by yellow lines). RNAP II, shown in black, enter the gene and form pelotons over a distance of a few hundred base pairs. **B)** The RNAP II density, RNAP II velocity, and nucleosome density corresponding to the kymograph in A). Simulations (supplementary files **Figure5-sourcedata1** and **Figure5-sourcedata2**) where averaged over the size of a nucleosome and are shown as black dots and our analytical predictions as red lines. The velocity in the simulations was determined by dividing the motor flux by the average motor density. **C)** Kymograph for relatively high initiation rates, resulting in larger pelotons as compared to A). **D)** The RNAP II density, RNAP II velocity, and nucleosome density corresponding to the kymograph in B). Comparing B) and D), we see that larger pelotons give a visibly stronger density and velocity evolution.

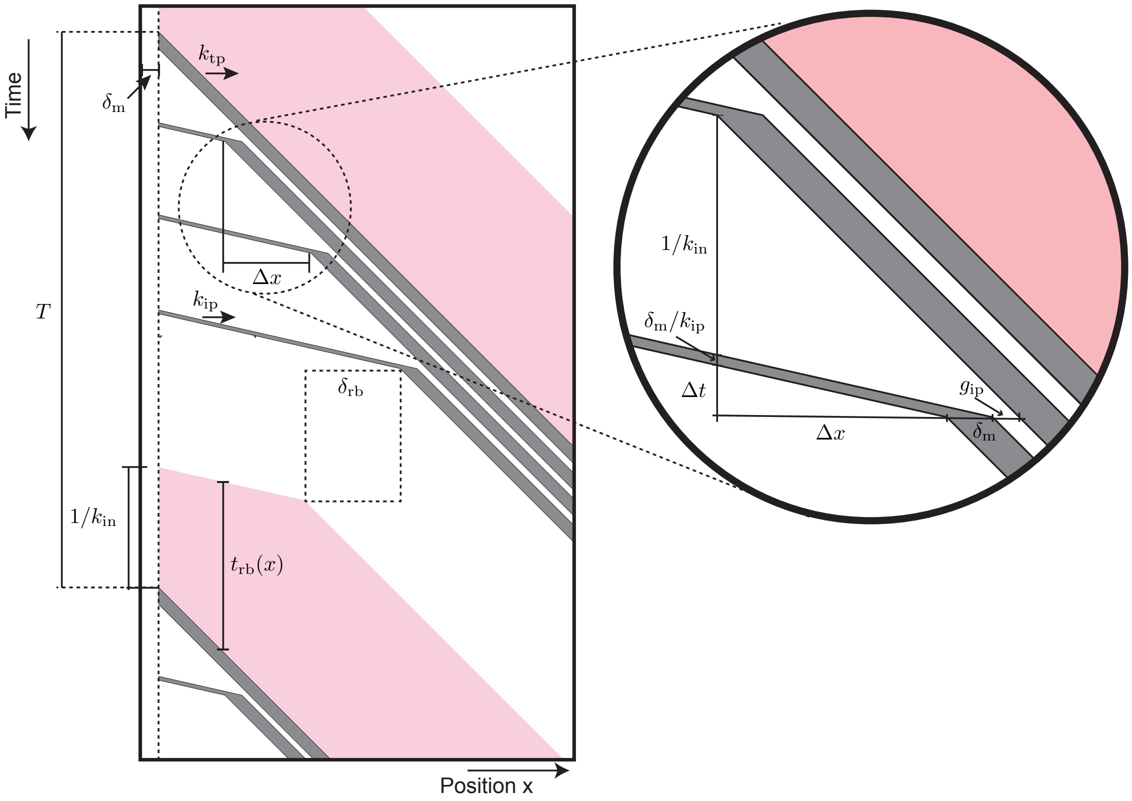
Time
δ_{m}
k_{tp}
Δx
k_{ip}
T
δ_{rb}
$1/k_{\mathrm{in}}$
$t_{\mathrm{rb}}(x)$
Position x
$1/k_{\mathrm{in}}$
$\delta_{\mathrm{m}}/k_{\mathrm{ip}}$
Δt
g_{ip}
Δx
δ_{m}

Figure 6: A schematic kymograph of the system with open boundary conditions. Motors (grey) initiate on the left side of the lattice, with an initiation site free of roadblocks. As motors travel into the system, their speed depends on if there is a roadblock (pink) ahead of them. With a roadblock ahead, the motor speed is k_{tp}, while without roadblock ahead it is k_{ip}. The typical time that a roadblock at position x is bound before being evicted by the next peloton is given by $t_{\mathrm{rb}}(x)$. The right figure is a magnification of the region defining Δx, which is the typical distance a motor travels to catch up with the proto peloton since the last motor caught up

Tables

Table 1: Parameter values as estimated from the literature and implemented in the simulations.

Microscopic parameter	Value	Citation
RNAP II footprint (δ_{m})	35 bp	(Greive and Hippel, 2005)
Nucleosome (147bp) + linker DNA (20 bp)= (δ_{rb})	167 bp	(Brogaard et al., 2012; Luger et al., 1997)
Elongation rate on bare DNA (including pausing) (k_{ip})	10 bp/s	(Bintu et al., 2012; Darzacq et al., 2007)
Elongation rate through nucleosome (k_{tp})	3 bp/s	(Bintu et al., 2012)
Initiation rate on typical and highly transcribed genes (k_{in})	0.6-3/min	(Pelechano et al., 2010)
Roadblock equilibration time (τ) ≈ tetramer binding time	≈ 0	(Mazurkiewicz et al., 2006; Schwabish and Struhl, 2004; Worcel et al., 1978)

Table 2: Calculated observables for the physiological parameters in **Table 1**

k_{in}	0.6 pol/min	3.0 pol/min
v^{in}	5.5 bp/s	8.1 bp/s
J	0.6 pol/min	2.3 pol/min
$\rho_{\text{m}}^{\text{in}}$	0.002 pol/bp	0.006 pol/bp
$\langle n_{\text{p}} \rangle^*$	1.6 pol	3.8 pol
ρ_{m}^*	0.003 pol/bp	0.013 pol/bp
x^*	420 bp	280 bp
k_{on}	1.1/min	1.1/min
k_{tr}	1.8/min	3.8/min
k_{off}	3.3/min	1.4/min